Heliyon 9 (2023) e22200

Contents lists available at ScienceDirect

Heliyon

journal homepage: www.cell.com/heliyon

An anoikis-related lncRNA signature is a useful tool for predicting the prognosis of patients with lung adenocarcinoma

Xin Jiang [a,b,1], Yu-lu Gao [d,1], Jia-yan Li [a,b], Ying-ying Tong [a], Zhao-yang Meng [c], Shi-gui Yang [e,**], Chang-tai Zhu [b,*]

[a] College of Fisheries and Life Science, Shanghai Ocean University, Shanghai, 201306, China
[b] Department of Transfusion Medicine, Shanghai Sixth People's Hospital Affiliated to Shanghai Jiao Tong University School of Medicine, Shanghai, 200233, China
[c] Department of Pharmacy, Shanghai Sixth People's Hospital Affiliated to Shanghai Jiao Tong University School of Medicine, Shanghai, 200233, China
[d] Department of Laboratory Medicine, Kunshan Affiliated Hospital of Nanjing University of Chinese Medicine, Kunshan, 215300, China
[e] Department of Public Health, Zhejiang University School of Medicine, Hangzhou, 310000, China

ARTICLE INFO

Keywords:
Lung adenocarcinoma
LncRNA
Anoikis
Prognostic signature

ABSTRACT

Background: Anoikis-related long non-coding RNAs (ARLs) play a critical role in tumor metastasis and progression, suggesting that they may serve as risk markers for cancer. This study aimed to investigate the prognostic value of ARLs in patients with lung adenocarcinoma (LUAD).

Methods: Clinical data, RNA sequencing (RNA-seq) data, and mutation data from the LUAD project were obtained from The Cancer Genome Atlas (TCGA) database. The Molecular Signatures Database (MSigDB) and the GeneCard database were used to collect an anoikis-related gene (ARG) set. Pearson correlation analysis was performed to identify ARLs. LASSO and Cox regression were then used to establish a prognostic risk signature for ARLs. The median risk score served as the basis for categorizing patients into high and low-risk groups. Kaplan-Meier analysis was utilized to compare the prognosis between these two groups. The study also examined the associations between risk scores and prognosis, clinicopathological characteristics, immune status, tumor mutation burden (TMB), and chemotherapeutic agents. LncRNA expression was assessed using quantitative real-time PCR (qRT-PCR).

Results: A total of 480 RNA expression profiles, 501 ARGs, and 2698 ARLs were obtained from the database. A prognostic ARL signature for LUAD was established, consisting of 9 lncRNAs. Patients in the low-risk group exhibited significantly better prognosis compared to those in the high-risk group ($P < 0.001$). The 9 lncRNAs from the ARL signature were identified as independent prognostic factors ($P < 0.001$). The signature demonstrated high accuracy in predicting LUAD prognosis, with area under the curve values exceeding 0.7. The risk scores for ARLs showed strong negative correlations with stroma score ($P = 5.9E-07$, $R = -0.23$), immune score ($P = 9.7E-09$, $R = -0.26$), and microenvironment score ($P = 8E-11$, $R = -0.29$). Additionally, the low-risk group exhibited significantly higher TMB compared to the high-risk group ($P = 4.6E-05$). High-risk status was significantly associated with lower half-maximal inhibitory concentrations for most chemotherapeutic drugs.

* Corresponding author.
** Corresponding author.
E-mail addresses: yangshigui@zju.edu.cn (S.-g. Yang), zct101@163.com (C.-t. Zhu).
[1] Equal contributors.

https://doi.org/10.1016/j.heliyon.2023.e22200
Received 25 May 2023; Received in revised form 15 August 2023; Accepted 6 November 2023
Available online 11 November 2023

Conclusion: This newly constructed signature based on nine ARLs is a useful instrument for the risk stratification of LUAD patients. The signature has potential clinical significance for predicting the prognosis of LUAD patients and guiding personalized immunotherapy.

1. Introduction

Lung cancer is a primary malignancy of the lung, and it has the highest mortality and morbidity rates among all cancers [1], with approximately 1.76 million deaths and 2 million new cases each year [2]. A major type of lung cancer is lung adenocarcinoma (LUAD), which has extremely low patient survival rates [3]. Although surgical excision is still the preferred method of radical treatment in the early stages of LUAD [4], and significant efforts have been made to develop new therapies, patient prognosis remains poor [5]. Conventional bronchoscopy and computed tomography are inadequate for detecting early-stage LUAD [6], and even timely treatment with targeted therapies, radiotherapy, and surgery cannot change the highly lethal nature of LUAD [7]. Therefore, there is a great need for new effective methods of LUAD diagnosis, as well as the identification of molecular features associated with patient survival. This will help in the development of more effective prognostic biomarkers for LUAD.

Cells undergo mutual interactions with adjacent cells and the extracellular matrix (ECM) [8]. A lack of proper cell/ECM attachment causes a type of programmed cell apoptosis called anoikis [9–11]. Anoikis prevents the re-adhesion of dislodged cells to incorrect locations and blocks their subsequent growth [10], which supports the removal of dislodged or misplaced cells to maintain tissue homeostasis. Anoikis is involved in a variety of pathological mechanisms, including oncogenic effects. Cancer cells detach from other cancer cells and the ECM, metastasize, and attach to new sites. Subsequent proliferation at these new sites results in the diffusion of the tumor and greatly worsens the patient's prognosis [12].

Anoikis serves as a crucial physiological barrier that is activated by the rapid activation of cell surface death receptors or disruption of the mitochondrial pathway [13,14]. Nevertheless, cancer cells possess the ability to evade anoikis, thus enabling them to detach from their primary site and metastasize through various mechanisms. These mechanisms include altering the expression patterns of cellular integrins, activating pro-survival signaling pathways, and secreting growth factors [15]. By doing so, cancer cells are able to evade death signaling pathways after detachment from the primary site [16] and spread through the circulatory and lymphatic systems [17]. Anoikis resistance plays a significant role in tumor development and is considered an emerging marker of tumor cells [18,19]. In the context of lung cancer, anoikis resistance is achieved through the TGF-β1/SH2B3 axis, which modulates the SHP2/Grb2 and JAK2/STAT3 signaling pathways [20]. Additionally, the binding of MTHFD1 and PRMT5 has been found to be associated with cancer metastasis and increased resistance to anoikis. This binding enhances the arginine methylation modification of MTHFD1, leading to a significant increase in the metabolic activity of NADPH [21]. Furthermore, recent studies have demonstrated that the interregulation of SMAD1-SMAD3 and SOX2 is crucial for cancer metastasis and resistance to anoikis [22]. In summary, anoikis-related genes (ARGs) play a critical role in tumor development; however, there is a lack of systematic studies that have reviewed the impact of anoikis-related long non-coding RNAs (ARLs) on the prognosis of patients with LUAD.

Long non-coding RNAs (lncRNAs) exhibit diverse sequences, structures, and functions [23], ranging in length from 200 nt to approximately 100,000 bases [24]. Through their multifaceted functions [25], lncRNAs can regulate nucleosome assembly and functions, control chromatin activities, directly bind to target RNAs to modulate translation or stability [26], and interfere with signaling pathways, thereby participating in gene regulation [27]. As crucial regulatory molecules, lncRNAs play a pivotal role in various biological processes, including apoptosis, cell migration, cell proliferation, and metabolic regulation, operating through diverse pathways [28], particularly during tumorigenesis [29]. Consequently, dysregulated lncRNAs hold potential as prognostic biomarkers for tumors [30]. Numerous studies have highlighted the significant roles of lncRNAs in cancer development, such as MALAT1 in LUAD [31], RMRP in bladder cancer [32], TLNC1 in liver cancer [33], and HOXA10-AS in oral cancer [34]. Given the pivotal functions of lncRNAs in tumors, they represent promising targets for precision tumor therapy. Therefore, it is crucial to further investigate the roles of ARLs in LUAD.

In this study, our objective is to explore the prognostic value of ARL in LUAD and develop a novel ARL signature using LUAD data from The Cancer Genome Atlas (TCGA). Our research will provide valuable insights into effective prognostic biomarkers and potential therapeutic strategies for LUAD.

2. Materials and methods

2.1. Datasets and preprocessing

Mutation data, clinical data, and RNA-seq data for 480 cases of LUAD were downloaded from the TCGA repository (https://portal.gdc.cancer.gov/repository) as of November 2022. Transcripts per kilobase of exon model per million mapped reads (TPM) data and fragments per kilobase of exon model per million mapped fragments (FPKM) data from RNA-seq were extracted using the Perl language (version 5.30.0.1), and the lncRNAs> matrix was also extracted from the RNA-seq dataset. A total of 501 ARGs were identified from MSigDB (https://www.gsea-msigdb.org/gsea/) and GeneCard (https://www.genecards.org/) as of November 2022.

2.2. Differential gene expression and functional enrichment analysis

The "limma" package (Ritchie et al., 2015) in R software (version 4.2.0) was used to filter out differentially expressed ARGs, with the screening thresholds set to FDR <0.05 and $|\log2FC| > 1$. Then, differentially expressed genes (DEGs) related to anoikis were analysed using the "clusterProfiler" package for Gene Ontology (GO) and Kyoto Encyclopedia of Genes and Genomes (KEGG) analysis.

2.3. Construction of the ARG LncRNA predictive signature

The correlations between ARGs and lncRNAs were analysed using the "limma" package. The filtering criteria were set using the correlation coefficient ($P < 0.001$ and $R^2 > 0.4$). A total of 2698 ARLs were screened. Based on the screened ARLs, we first obtained prognosis-associated ARLs from LUAD patients using univariate Cox regression and then performed LASSO regression to eliminate overfitting lncRNAs. Finally, multivariate Cox regression was used to construct a prognostic signature for ARLs. The risk score was computed with the following formula:

$$\text{Risk score} = \sum_{i=1}^{n}(\text{coefficient lncRNA}_n \times \text{lncRNA}_n \text{ expression})$$

For more in-depth analysis, we computed the risk score of all LUAD patients using the risk score formula, and used the median risk score as the cutoff value to categorise the LUAD patients into high-risk and low-risk groups. Risk score distribution, survival status, and lncRNA expression heatmaps were plotted.

2.4. Construction of the mRNA–LncRNA network

According to the correlations between ARGs and lncRNAs, the regulatory network of mRNAs-lncRNAs was generated by using Perl software and Cytoscape software (version 3.6.1) based on the identified anoikis prognosis-associated lncRNAs with mRNAs, and the network relationships were visualized using Sankey diagrams with the "galluvial" package.

2.5. Construction of the nomogram

Univariate and multivariate Cox regression analyses were conducted to assess the impact of clinical traits such as stage, sex, and age. Based on the independent predictor variables, a predictive nomogram was constructed using the "rms" package. The reliability of the nomogram was evaluated through receiver operating characteristic (ROC) and calibration curves. Additionally, LUAD patients were categorized for survival analysis and multivariate ROC curve analysis, considering different clinical traits, to further explore the associations between these traits and the risk score.

2.6. Validation of the predictive signature

To assess the applicability of the predictive signature in the complete LUAD dataset, the 480 LUAD patients were randomly divided into two cohorts at a 1:1 ratio. Risk assessment analysis based on the risk score formula was performed on the two internal validation sets, followed by ROC curve analysis and survival analysis.

2.7. Gene set enrichment analysis (GSEA)

For further functional analysis of the two risk groups, GSEA software (version 4.2.3) was utilized. The analysis focused on two gene sets, namely "KEGG" and "GO". The "phenotype labels" option was set as "high-risk than low-risk", the "number of permutations" was set to "1000″, and all other settings were kept as default. The filtering condition was set as "FDR <0.25, NOM P value < 0.05".

2.8. Immune analysis of the signature

To assess immune infiltration, various algorithms including MCPCOUNTER, EPIC, TIMER, QUANTISEQ, CIBERSORT-ABS, CIBERSORT, and XCELL were employed. Immune scores, tumor microenvironment scores, and stromal scores were also calculated using xCELL. Additionally, we analysed the correlations between prognostic features and immune checkpoints such as BTLA, ICOS, CTLA4, and CD274 in different risk groups.

2.9. Mutation status analysis of the signature

To further understand the immunological nature of the risk scores, mutation analysis was performed separately for each risk group. Firstly, tumor mutation burden (TMB) analysis was conducted using the "maftools" package to identify mutated genes and explore their interactions. Secondly, the associations between risk scores, TMB, and patient prognosis were investigated using the "survminer" and "survivor" packages for survival analysis.

2.10. Chemotherapy drug response

Chemotherapy remains a more effective treatment for patients with advanced LUAD. To investigate sensitivity (IC50) to chemotherapy agents in the risk groups, drug response information was obtained from Genomics of Drug Sensitivity in Cancer (GDSC), and the "pRRophetic" package in R (version 4.1.0) was applied to predict the effect of chemotherapy drugs on each patient in the two different risk groups.

2.11. Cell culture and qRT-PCR

HBE cells were cultured in KM medium (ScienCell Research Laboratories, Carlsbad, CA, USA), A549 cells were cultured in DMEM (Gibco, Invitrogen Carlsbad, CA, USA) with 10% fetal bovine serum (FBS), and H1299 cells were cultured in RPMI-1640 medium (Gibco) with 10% FBS. All cells were incubated at 37 °C with 5% CO2. Total RNA was extracted using TRIzol reagent (Invitrogen) and evaluated using a multifunctional enzyme marker SpectraMax® i3x (Molecular Devices, Shanghai, China). The PrimeScript™ RT Reagent Kit with gDNA Eraser (TaKaRa, Dalian, Liaoning, China) was used for reverse transcription of RNA to synthesize cDNA. cDNA was then synthesized using TB Green® Premix Ex Taq™ (TaKaRa) on a LightCycler® 480II (Roche Diagnostics Ltd., Rotkreuz, Switzerland), with GAPDH serving as an internal control for qRT-PCR. The relative expression levels of lncRNA were determined in triplicate using the $2^{-\triangle\triangle}$Ct method. The primer sequences used in this study are provided in Supplemental File 1.

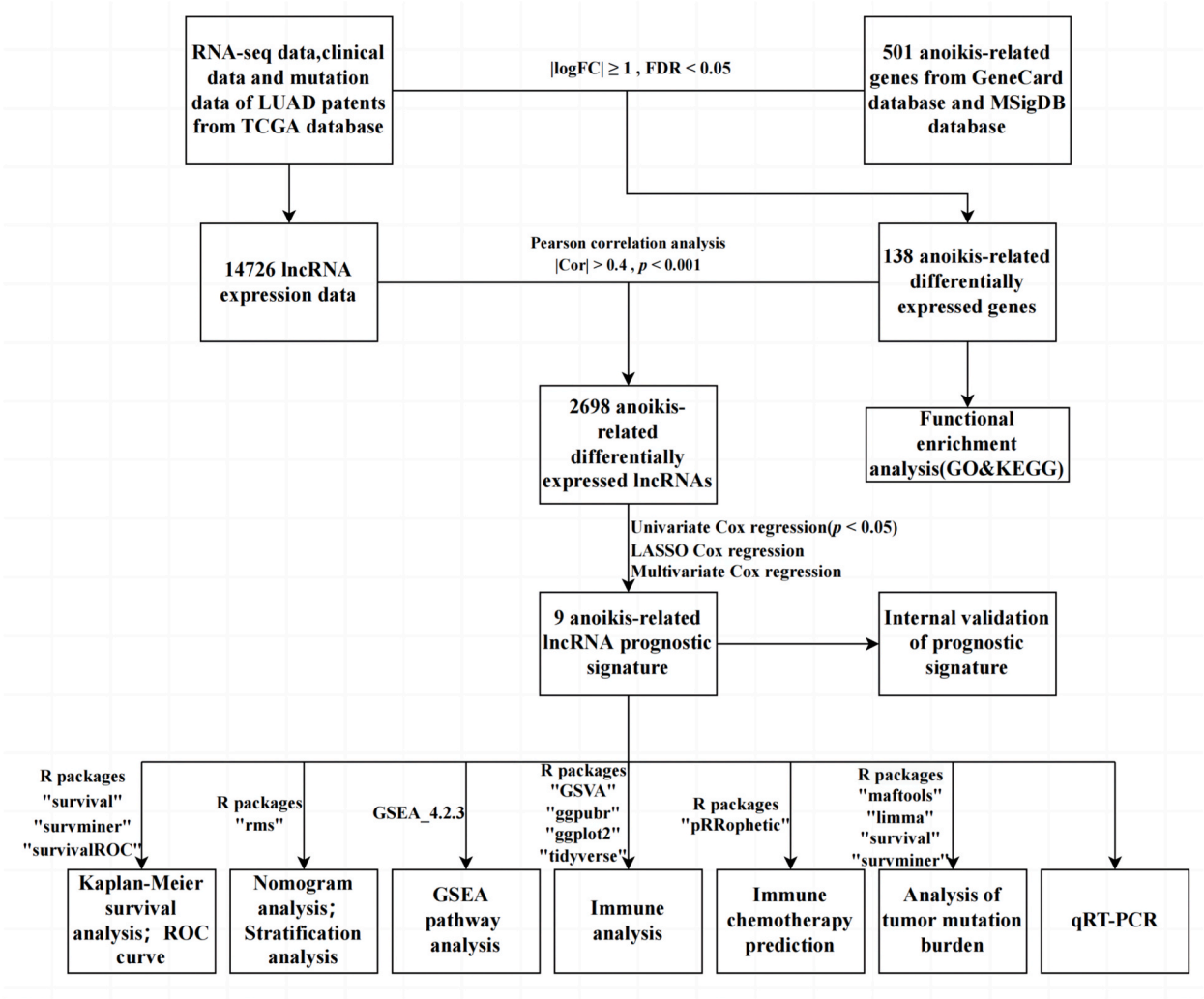

Fig. 1. Overall flowchart of the study.

2.12. Statistical analysis

Statistical analysis and data visualization were performed using R software (versions 4.1.0 & 4.2.0), Perl language (version 5.30.0.1), and GraphPad Prism software (version 8.0.2). T-tests and one-way ANOVA were used for parametric data analysis. The chi-square test was used to compare differences between high-risk and low-risk groups. Survival analysis was conducted using the Kaplan-Meier method and log-rank tests. LASSO Cox regression analysis was employed to establish the ARL prognostic signature. A p-value of <0.05 was considered statistically significant unless otherwise specified.

3. Results

3.1. Differential gene expression and functional enrichment analysis

Fig. 1 illustrates the workflow diagram for this study. Through differential analysis, we identified 138 differentially expressed genes (DEGs) related to anoikis (Fig. 2A), with 103 genes upregulated and 35 genes downregulated. KEGG pathway analysis revealed that the anoikis DEGs were primarily enriched in focal adhesion, prostate cancer, fluid shear stress and atherosclerosis, microRNAs in cancer, the cell cycle, bladder cancer, melanoma, ECM-receptor interaction, the IL-17 signaling pathway, and the PI3K-Akt signaling pathway (Fig. 2B). GO analysis demonstrated that the DEGs were mainly enriched in the regulation of protein serine/threonine kinase activity,

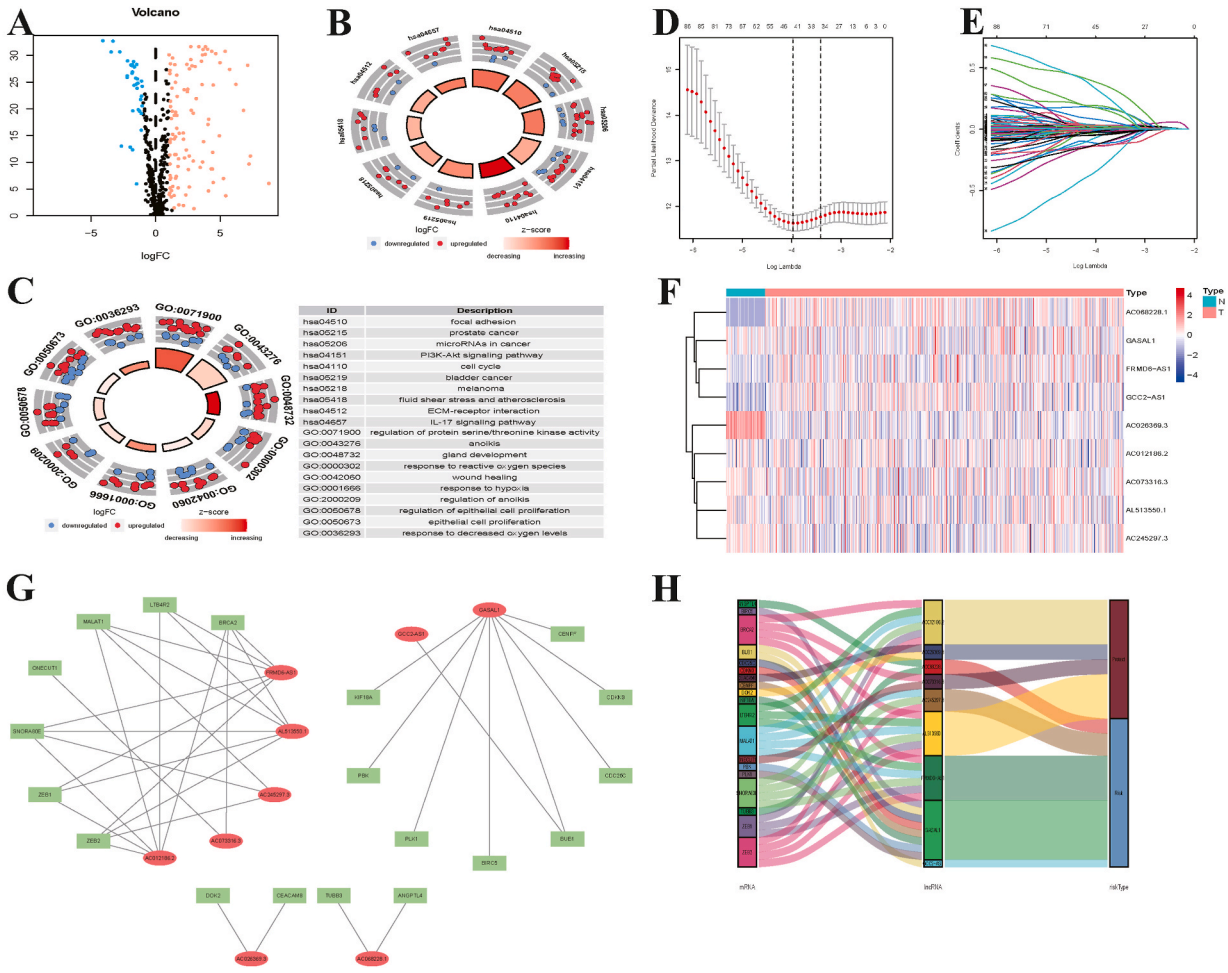

Fig. 2. Identification of an anoikis-related lncRNA signature to predict the prognosis of patients with LUAD. **(A)** Volcano diagram shows the differentially expressed genes with the threshold set at FDR <0.05 and $|\log2FC| > 1$. **(B)** Loop diagram of KEGG analysis of anoikis-associated DEGs. log2FC > 1 for upregulated, log2FC < 1 for downregulated. **(C)** Loop diagram of GO analysis of anoikis-associated DEGs. The outer circle shows a scatter diagram of each term's log fold change (FC) value. log2FC > 1 for upregulated, log2FC < 1 for downregulated. **(D)** Distribution plot of the partial likelihood deviation from the LASSO regression. **(E)** Cross-validation for tuning parameter selection in the LASSO regression. **(F)** The expression levels of nine anoikis-related lncRNAs in LUAD and normal tissues. **(G)** Prognostic coexpression network of the nine anoikis-related lncRNAs and mRNAs. **(H)** Sankey diagram of the relationship between lncRNAs and mRNAs. KEGG, Kyoto Encyclopedia of Genes and Genomes; GO, Gene Ontology; DEGs, differentially expressed genes; FDR, false discovery rate; FC, fold change; N, normal; T, tumor.

anoikis, gland development, the response to reactive oxygen species, wound healing, the regulation of anoikis, the response to hypoxia, the regulation of epithelial cell proliferation, the response to decreased oxygen levels, and epithelial cell proliferation (Fig. 2C).

3.2. Construction of the anoikis-related LncRNA predictive signature

A total of 2698 anoikis-related lncRNAs (ARLs) were screened based on the calculated correlations. Univariate Cox regression analysis identified 98 ARLs associated with prognosis in LUAD patients, and LASSO regression further narrowed it down to 43 prognosis-related ARLs (Fig. 2D–E). Finally, 9 prognosis-related ARLs (AC012186.2, GASAL1, AC073316.3, AC068228.1, AL513550.1, AC026369.3, FRMD6-AS1, GCC2-AS1, and AC245297.3) were selected to construct a predictive signature (Table 1). The expression levels of these 9 ARLs are shown in the heatmap (Fig. 2F). According to the mRNA-lncRNA regulatory network map (Fig. 2G), AC012186.2/AL513550.1/FRMD6-AS1 were coexpressed with 6 ARGs (ZEB2, ZEB1, SNORA80E, MALAT1, LTB4R2, and BRCA2), GASAL1 was coexpressed with 8 ARGs (KIF18A, PBK, PLK1, BIRC5, BUB1, CDC25C, CDKN3, and CENPF), AC073316.3 was coexpressed with 2 ARGs (ONECUT1 and BRCA2), AC068228.1 was coexpressed with 2 ARGs (TUBB3 and ANGPTL4), AC026369.3 was coexpressed with 2 ARGs (DOK2 and CEACAM8), GCC2-AS1 was coexpressed with one ARG (BUB1), and AC245297.3 was coexpressed with 3 ARGs (ZEB2, SNORA80E, and ALAT1). Based on the hazard ratio values from multifactorial Cox regression analysis and the mRNA-lncRNA regulatory network, the "galluvial" package was used to plot the Sankey diagram (Fig. 2H), which revealed that AC012186.2, AC073316.3, AL513550.1, and AC026369.3 were protective factors, while GASAL1, AC068228.1, FRMD6-AS1, GCC2-AS1, and AC245297.3 were risk factors.

Afterwards, the risk scores for each patient with LUAD were calculated using a specific formula, and then the patients were divided into high-risk and low-risk groups based on the median value of their risk scores. To assess the predictive value of these risk scores on the prognosis of LUAD patients, Kaplan-Meier analysis was employed to analyze the overall survival (OS) and progression-free survival (PFS) times in both the high-risk and low-risk groups. The OS and PFS curves (Fig. 3A–B) clearly demonstrate that the survival rates were significantly better in the low-risk group compared to the high-risk group ($P < 0.001$), and mortality increased as the risk scores increased (Fig. 3C–D). The ROC curve analysis yielded area under the curve (AUC) values of 0.741, 0.753, and 0.77 at 1, 3, and 5 years, respectively (Fig. 3E), indicating the accuracy of the prognostic predictions made by the signature.

3.3. Construction of a predictive nomogram

Univariate and multivariate Cox regression analyses were performed by combining clinicopathological traits with the risk scores. The univariate Cox regression analysis revealed that the risk scores, T/N stage, and stage were all significantly associated with prognosis (Fig. 3F), while the multivariate Cox regression analysis showed that the risk scores and stage remained significantly correlated with prognosis (Fig. 3G), suggesting that the ARLs used in our signature can serve as independent prognostic factors. To further enhance the predictive power of these ARLs, clinical factors were integrated with the ARL signature to create a nomogram (Fig. 3H). The calibration curves for 1-, 2-, 3-, and 5-year survival times demonstrated the prognostic value of this nomogram (Fig. 3I-L).

3.4. Correlations between various clinicopathological traits of LUAD and risk scores

To further investigate the correlations between various clinicopathological traits and risk scores, LUAD patients were grouped based on different clinicopathological traits for survival analysis and multivariate ROC curve analysis. The multivariate ROC curves revealed that the ARL signature had a much higher AUC than other clinical traits (Fig. S1A). The risk curves for different clinical characteristics also showed that the OS in the high-risk group was significantly worse than that in the low-risk group (Figs. S1B–E).

3.5. Validation of the predictive signature

The clinicopathological traits of LUAD patients are shown in Table 2. Consistent with the results for the complete dataset, the number of deaths in each internal cohort was proportional to the risk score (Fig. 4A–B, E-F). In both internal cohorts, the low-risk score

Table 1
The assiciation of anoikis-related lncRNAs signature with the prognosis of patients with lung adenocarcinoma.

lncRNA	Coefficient	HR	HR (95% CI)	*P*
AC012186.2	−0.63	0.53	0.34–0.82	0.004251
GASAL1	0.38	1.46	0.93–2.32	0.103305
AC073316.3	−0.48	0.62	0.36–1.04	0.071933
AC068228.1	0.41	1.50	1.05–2.16	0.027706
AL513550.1	−0.58	0.56	0.39–0.80	0.001609
AC026369.3	−0.20	0.82	0.65–1.03	0.094031
FRMD6-AS1	0.81	2.26	1.24–4.09	0.007383
GCC2-AS1	0.55	1.74	0.99–3.06	0.055569
AC245297.3	0.49	1.63	1.06–2.51	0.025193

HR: hazard ratio. CI: confidence interval.

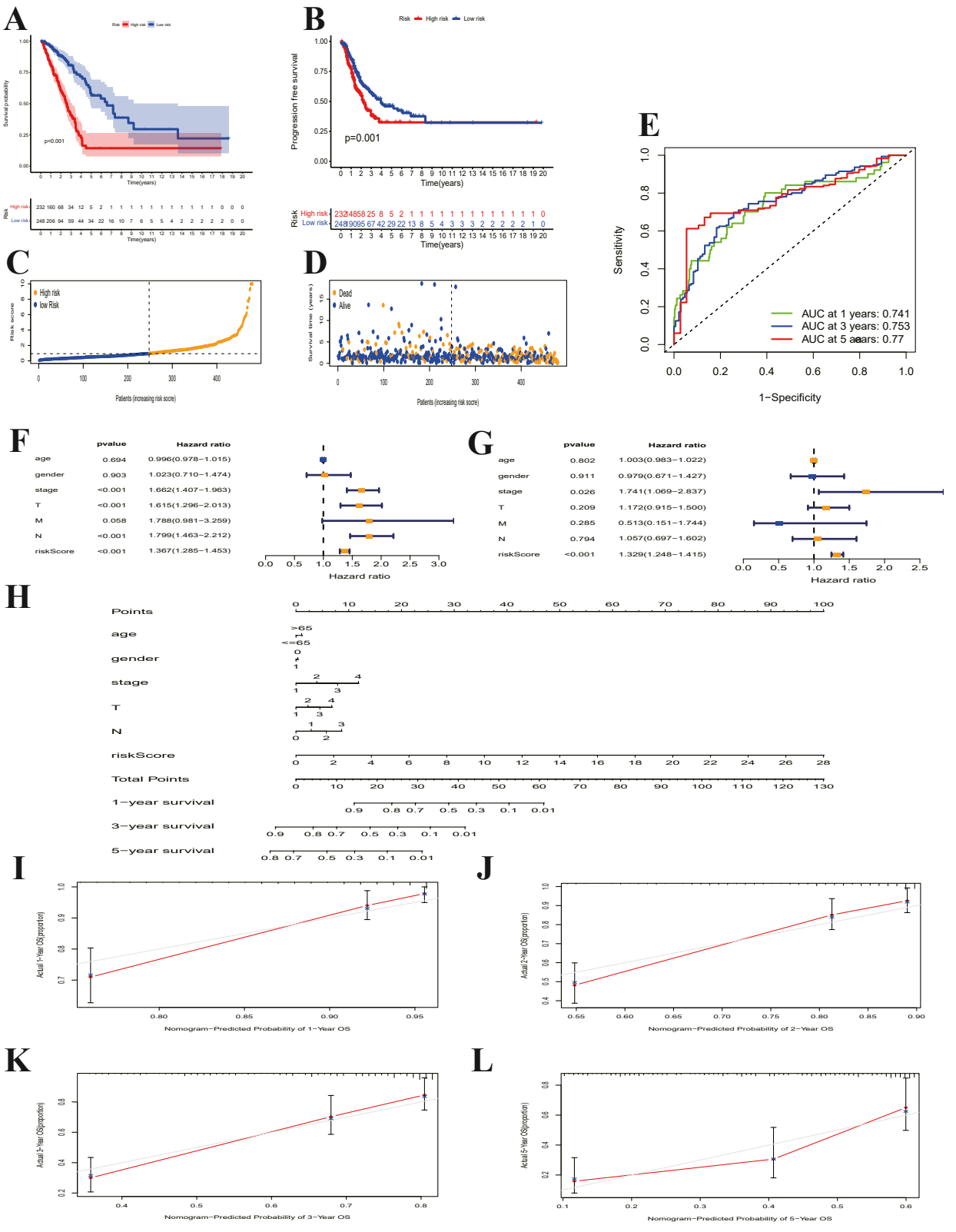

(caption on next page)

Fig. 3. Construction of a model based on the anoikis-related lncRNA signature to predict the prognosis of patients with LUAD. **(A-B)** Kaplan–Meier analysis of the OS and PFS rates of LUAD patients in the high- and low-risk groups. **(C-D)** Distribution of risk scores and survival status for the predictive signature. **(E)** Time-dependent ROC analysis of the predictive signature. **(F-G)** Forest plot for univariate and multivariate Cox regression analyses. **(H)** The nomogram predicts the probability of 1, 3, and 5 years of OS. **(I-L)** The calibration curves test consistency between the actual OS rates and the predicted survival rates at 1, 2, 3, and 5 years. AUC, area under the curve; T, tumor; M, metastasis; N, lymph node.

Table 2
Clinicopathological characteristics of the LUAD patient.

Clinicopathological Variables	Entire TCGA cohort (n = 480)	First cohort (n = 240)	Second cohort (n = 240)
Age (years)			
≤ 65	231 (48.13%)	114 (47.5%)	117 (48.75%)
>65	249 (51.88%)	126 (52.5%)	123 (51.25%)
Gender			
Female	259 (53.96%)	122 (50.83%)	137 (57.08%)
Male	221 (46.04%)	118 (49.17%)	103 (42.92%)
Stage			
Stage I	255 (53.13%)	123 (51.25%)	132 (55.00%)
Stage II	114 (23.75%)	60 (25.00%)	54 (22.50%)
Stage III	78 (16.25%)	38 (15.83%)	40 (16.67%)
Stage IV	25 (5.20%)	15 (6.25%)	10 (4.17%)
Unknow	8 (1.67%)	4 (1.67%)	4 (1.67%)
T			
T1	160 (33.33%)	73 (30.42%)	87 (36.25%)
T2	256 (53.33%)	130 (54.17%)	126 (52.50%)
T3	43 (8.96%)	24 (10.00%)	19 (7.92%)
T4	18 (3.75%)	11 (4.58%)	7 (2.92%)
TX + unknow	3 (0.63%)	2 (0.83%)	1 (0.42%)
M			
M0	316 (65.83%)	161 (67.08%)	155 (64.58%)
M1	24 (5.00%)	14 (5.83%)	10 (4.17%)
MX + unknow	140 (29.17%)	65 (27.08%)	75 (31.25%)
N			
N0	309 (64.38%)	154 (64.17%)	155 (64.58%)
N1	91 (18.96%)	49 (20.42%)	42 (17.50%)
N2	67 (13.96%)	30 (12.50%)	37 (15.42%)
N3	2 (0.42%)	1 (0.42%)	1 (0.42%)
NX + unknow	11 (2.29%)	6 (2.50%)	5 (2.08%)
Risk score			
High	232 (48.33%)	120 (50.00%)	112 (46.67%)
Low	248 (51.67%)	120 (50.00%)	128 (53.33%)

T: tumor; N: node; M: metastasis.

group had significantly better survival rates (Fig. 4C, G). The ROC curves for both cohorts also indicated high accuracy for predicting prognosis, with AUCs of 0.757, 0.757, and 0.828 at 1, 3, and 5 years, respectively, for the first internal cohort (Figs. 4D), and 0.714, 0.756, and 0.736, respectively, for the second internal cohort (Fig. 4H).

3.6. Gene set enrichment analysis

In the top 10 GO analysis, several biological process (BP) terms were found to be significantly enriched in the group with high-risk scores. These include meiotic cell cycle process, nuclear chromosome segregation, and positive regulation of cell cycle. Additionally, the molecular function (MF) term cadherin binding and the cellular component (CC) term condensed chromosome were also significantly enriched in this group. On the other hand, the group with low-risk scores showed significant enrichment in BP terms such as activation of Janus kinase activity, leukotriene biosynthetic process, positive regulation of neuroinflammatory response, and response to macrophage colony-stimulating factor. The CC term MHC protein complex was also significantly enriched in this group (Figs. S2A–B).

Furthermore, the top five significantly enriched KEGG pathways in the high-risk score group were cell cycle, N glycan biosynthesis, ubiquitin-mediated proteolysis, p53 signaling pathway, and small cell lung cancer. In contrast, the top five significantly enriched KEGG pathways in the low-risk score group were primary bile acid biosynthesis, autoimmune thyroid disease, haematopoietic cell lineage, intestinal immune network for IgA production, and asthma (Figs. S2A–B).

3.7. Immunity analysis of the signature

To investigate the relationship between the signature and the tumor immune landscape, we performed an immune cell infiltration analysis using different algorithms. The results showed that the majority of immune cells from the tumor microenvironment (TME)

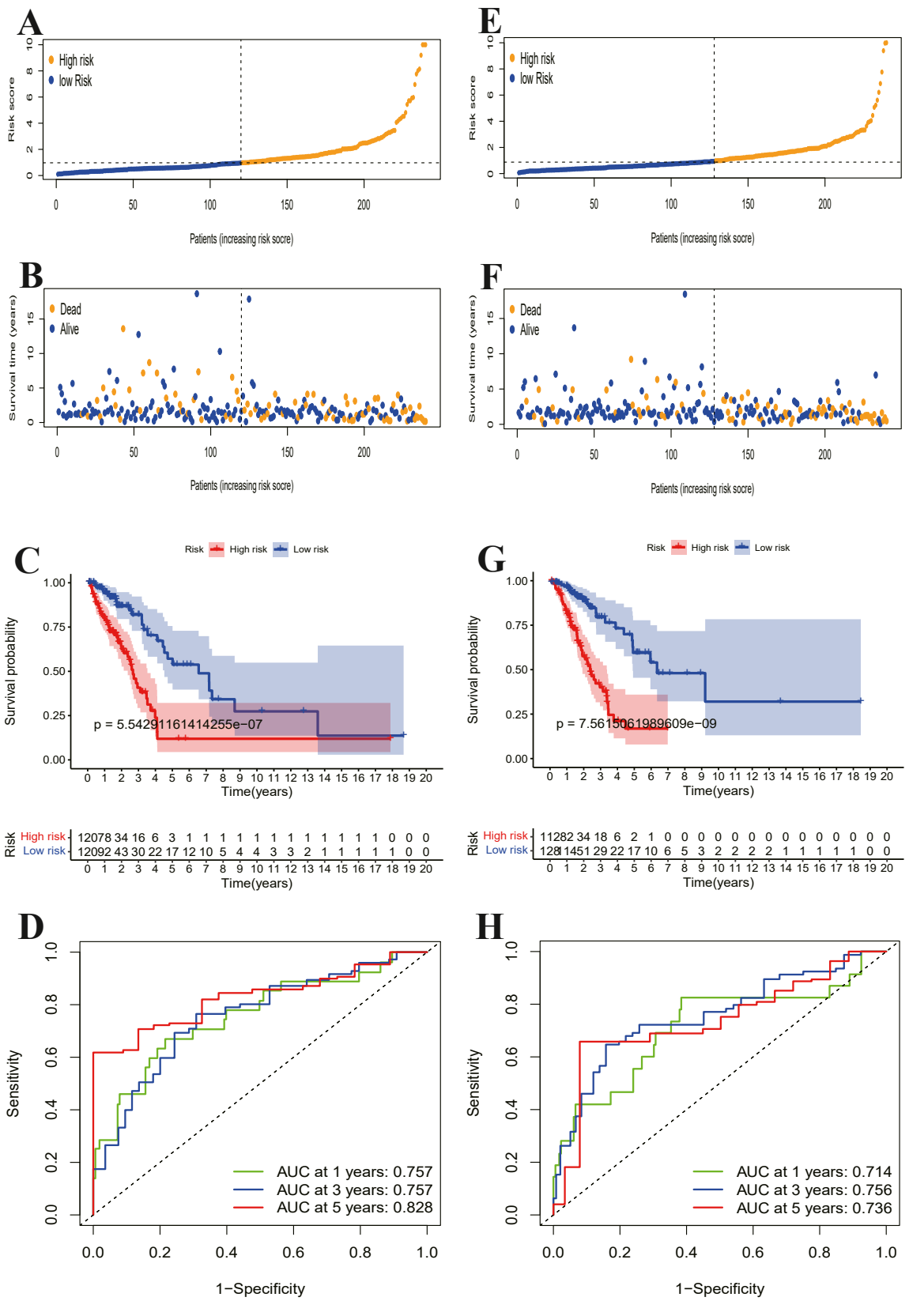

(caption on next page)

Fig. 4. Validation of the model based on the anoikis-related lncRNA signature for predicting the prognosis of patients with LUAD. **(A-B)** Distribution of risk scores and survival status for the first internal cohort. **(E-F)** Distribution of risk scores and survival status for the second internal cohort. **(C, G)** Kaplan–Meier survival curve for the first and second internal cohorts. **(D, H)** Time-dependent ROC analysis of the first and second internal cohorts. AUC, area under the curve.

were significantly correlated with high-risk scores (Fig. S3, Figs. S4A–I). Interestingly, the TME scores, stromal scores, and immune scores computed with the xCELL algorithm were higher in the low-risk score group (Fig. S4J-L).

Furthermore, we examined the expression levels of several immune-related genes. BTLA, ICOS, and CTLA4 showed lower expression levels in the group with high-risk scores, while the difference in CD274 expression was not significant (Fig. 5A–D).

3.8. Mutation analysis of the signature

Notably, 13 genes exhibited a higher frequency of mutations in the group with high-risk scores compared to the group with low-risk scores. These genes include COL11A1, ZNF536, NAV3, SPTA1, XIRP2, USH2A, ZFHX4, LRP1B, RYR2, CSMD3, MUC16, TTN, and TP53, with TP53 having the highest mutation frequency. Missense mutations were the most common type of mutations observed in both subgroups (Fig. 5E–F).

Furthermore, we conducted analysis on tumor mutational burden (TMB) and survival. We found that the high-TMB group had a better prognosis compared to the low-TMB group ($P = 0.014$), with the best prognosis observed in the group with low-risk scores and high TMB ($P < 0.001$) (Fig. 5G–H). Additionally, we compared TMB between the high and low-risk groups and found that TMB was higher in the high-risk score subgroup (Fig. 5I).

3.9. Chemotherapy drug response

Based on the IC50 values from the GDSC database, we identified several commonly used anticancer drugs, including cytarabine, cisplatin, doxorubicin, docetaxel, erlotinib, etoposide, gefitinib, gemcitabine, methotrexate, paclitaxel, and vinorelbine (Fig. 5J-T). Patients in the high-risk score group showed increased sensitivity to all of these anticancer drugs, except for methotrexate.

3.10. Validation of the LncRNAs in LUAD cells

Comparing LUAD cells to HBE cells, we observed significant downregulation of AC012186.2, AC068228.1, FRMD6-AS1, and AC245297.3, and marked upregulation of GCC2-AS1 and GASAL1. A549 cells showed significant downregulation of AL513550.1. qRT-PCR results confirmed that ARLs have high prognostic value for LUAD (Fig. 6A–G).

4. Discussion

ARGs play a critical role in cancer metastasis and invasion [35–37]. However, there have been limited studies that systematically evaluate the correlations between the prognosis of LUAD patients and ARLs. In our present study, we are the first to investigate and identify the relationships between ARLs and the prognosis of LUAD patients. Our prognostic signature, based on nine ARLs, demonstrates accurate prediction of outcomes for LUAD patients. Additionally, we have developed an ARL correlation nomogram model that provides a visual prediction of overall survival (OS) for LUAD patients. Importantly, the selected ARLs act as independent clinical prognostic factors and exhibit better predictive accuracy than individual clinical characteristics.

In our study, KEGG analysis was conducted on DEGs associated with anoikis. The results revealed several major enriched pathways, including focal adhesion, prostate cancer, fluid shear stress and atherosclerosis, microRNAs in cancer, bladder cancer, melanoma, the IL-17 signaling pathway, the PI3K-Akt signaling pathway, the cell cycle, and ECM-receptor interaction. Several studies have demonstrated the significance of focal adhesions in the progression of anoikis. Zhang et al. [38] conducted a comprehensive analysis to determine the impact of PCMT1 on cancer metastasis and focal adhesion kinetics, elucidating the drivers of anoikis resistance. Vivo et al. [39] discovered that focal adhesion kinase interacts with p14ARF to safeguard cells against anoikis. Hasnat et al. [40] observed that apigenin attenuates melanoma cell migration by inducing anoikis through integrin and focal adhesion kinase inhibition. Similarly, Enkhbat et al. [41] employed a colloidal self-assembled pattern to promote anoikis and p53 accumulation in A549 cells via focal adhesion. It is important to acknowledge the involvement of other enriched signaling pathways. For instance, Zhou et al. [42] revealed that AEG-1-dependent anoikis resistance is triggered through the PI3K/Akt pathway, which can be reversed by the PI3K inhibitor LY294002. Furthermore, Macabenta et al. [43] demonstrated that during collective mesenchymal migration, BMP-gated cell cycle processes drive anoikis. These studies have shed light on the pivotal roles of signaling pathways such as focal adhesion, cell cycle, and PI3K/Akt pathways in the process of anoikis, suggesting that ARGs may regulate the development of LUAD through these pathways. However, further comprehensive investigations are necessary to establish the association between ARGs and the development of LUAD.

We utilized LASSO regression and Cox regression analyses to construct predictive models involving nine ARLs (AC012186.2, GASAL1, AC073316.3, AC068228.1, AL513550.1, AC026369.3, FRMD6-AS1, GCC2-AS1, and AC245297.3). Notably, GASAL1 has been implicated in driving the progression of hepatocellular carcinoma by upregulating usp10, thereby stabilizing PCNA [44]. Additionally, the interaction between SRSF1 and GASAL1 has been identified as a regulator of apoptosis, invasion, and trophoblast

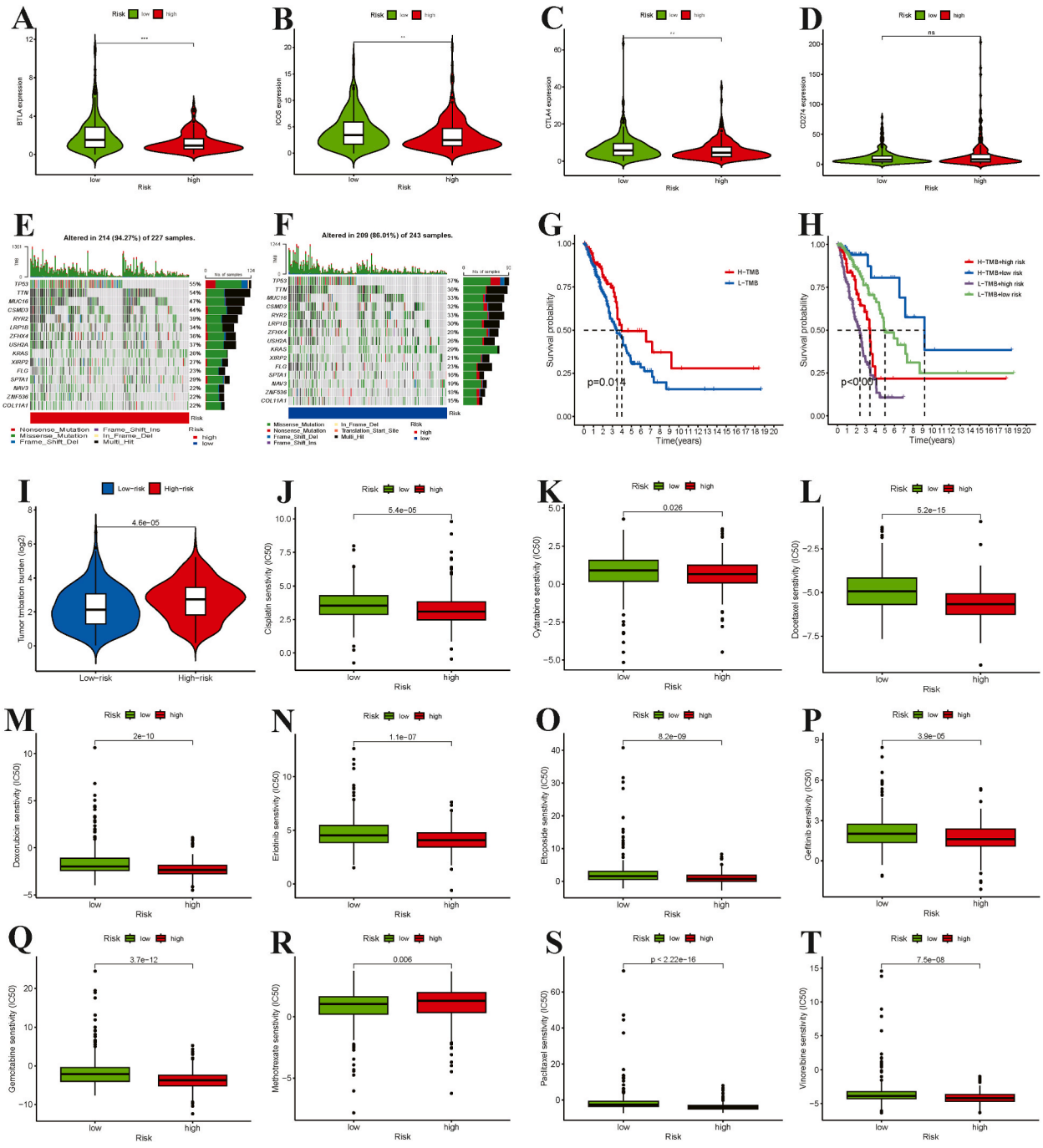

Fig. 5. Immune checkpoint analysis, gene mutation status analysis, and drug sensitivity analysis for the signature. **(A-D)** Expression levels of BTLA, ICOS, CTLA4, and CD274 in the high- and low-risk groups. **(E)** Top 15 gene mutations in the high-risk subgroup. **(F)** Top 15 gene mutations in the low-risk subgroup. **(G)** Kaplan–Meier survival curve of the high- and low-TMB groups. **(H)** Kaplan–Meier survival curve under the combined effect of risk score and TMB. **(I)** High and low TMB in the high- and low-risk groups. TMB, tumor mutation burden. **(J)** Cisplatin. **(K)** Cytarabine. **(L)** Docetaxel. **(M)** Doxorubicin. **(N)** Erlotinib. **(O)** Etoposide. **(P)** Gefitinib. **(Q)** Gemcitabine. **(R)** Methotrexate. **(S)** Paclitaxel. **(T)** Vinorelbine. IC50, half-maximal inhibitory concentration. *$p < 0.05$; **$p < 0.01$; ***$p < 0.001$; ns for no significance.

proliferation through the mTOR signaling pathway [45].

Furthermore, our findings were corroborated through in vitro experiments, where we validated the statistically significant differential expression profiles of seven lncRNAs, including GASAL1, in LUAD cells versus normal cells (HBE) using qRT-PCR. Collectively, these observations underscore the substantial role played by ARLs in the development of LUAD. It is important to note that the

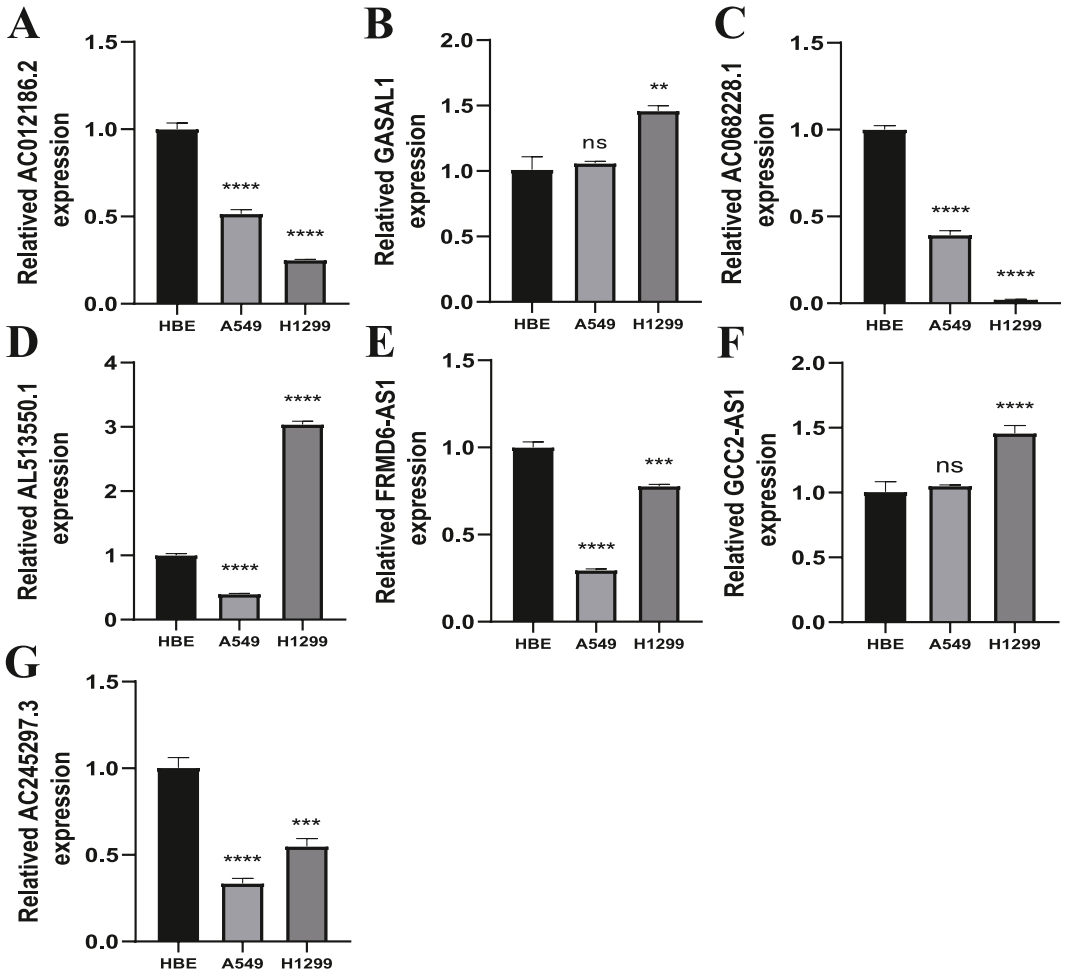

Fig. 6. The expression of anoikis-related lncRNAs in LUAD cells. **(A)** AC012186.2, **(B)** GASAL1, **(C)** AC068228.1, **(D)** AL513550.1, **(E)** FRMD6-AS1, **(F)** GCC2-AS1, and **(G)** AC245297.3 expression in normal (HBE) and LUAD cell lines. *$p < 0.05$; **$p < 0.01$; ***$p < 0.001$; ns for no significance.

precise regulatory mechanisms of these ARLs in LUAD necessitate further experimental exploration. It's worth mentioning that AC073316.3 and AC026369.3 were excluded from these experiments due to unsuccessful primer designs resulting in inadequate amplification and solubility curves.

Immunotherapy's impact on the prognosis of cancer patients is intricately intertwined with the regulation of cancer and immune cells within the tumor microenvironment (TME), a determinant of immunotherapy response [25]. Our study demonstrated a significant inverse association between most immune cells and high-risk scores. Notably, the low-risk score group displayed elevated stromal, tumor microenvironment, and immune scores compared to the high-risk score group. This observation suggests that risk scores effectively reflect the immune status of LUAD. Intriguingly, a substantial negative correlation emerged between pro-inflammatory immune cells (e.g., $CD8^+$ T-cells, $CD4^+$ T-cells, etc.) and regulatory immune cells (e.g., Tregs, M2 macrophages, etc.) with the risk score. This implies heightened immune activity within the low-risk group and, conversely, a relatively suppressed immune state in the high-risk group. Consequently, integrating these immune cell profiles with our ARL signature could enhance the accuracy of patient prognosis prediction.

Our investigation also explored the link between immune checkpoint-associated gene expression and the prognostic signature. The findings highlighted significantly lower expression of BTLA, ICOS, and CTLA4 in the high-risk group, suggesting their potential as targets for immune checkpoint therapy in LUAD patients. It's been proposed that TP53 could serve as an immune checkpoint inhibitor biomarker for LUAD [46,47]. In mutation analysis, we observed TP53's highest mutation frequency, with missense mutations being most prevalent in both risk score subgroups. Additionally, survival analysis of tumor mutation burden (TMB) revealed better survival in the high-TMB group, particularly among those with low-risk scores. This implies a strong connection between TP53 gene mutations and LUAD prognosis. However, in-depth research is needed to fully comprehend this relationship.

Finally, our signature was employed to predict drug sensitivity, identifying several common anticancer drugs. The outcomes underscored the promise of our prognostic signature as a predictor of anticancer drug response. Taken together, our signature emerges as a valuable resource for identifying therapeutic targets and immune biomarkers for LUAD patients.

However, our study is not without limitations. Firstly, the validation of our signature solely relied on TCGA data, and it is imperative to employ Gene Expression Omnibus data for result confirmation, including model performance evaluation. Secondly, we did not establish the reliability of our signature through in vivo experiments. Thirdly, our study lacked comprehensive experimental data elucidating the precise regulatory mechanisms of ARLs in LUAD. Thus, our future endeavors will delve deeper into understanding how ARLs contribute to the development of LUAD.

5. Conclusions

We developed a novel prognostic signature on the basis of ARLs. Further verification showed that this signature has potential value for predicting the prognosis of LUAD patients. Furthermore, our study provides insights for researchers exploring the regulatory mechanisms of anoikis in LUAD.

Funding

This work was supported by the Shanghai Pudong New Area Science and Technology Development Fund of China (PKJ2020-Y12).

Availability of data and materials

Most of the datasets used and/or analysed during the current study are publicly available from TCGA, GeneCard, and the Molecular Signatures Database (MSigDB). All data of the independent cohorts in the current study are available from the corresponding authors upon reasonable request.

Ethics approval and consent to participate

Review and/or approval by an ethics committee was not needed for this study because TCGA belongs to public databases, the patients involved in the database have obtained ethical approval. Users can download relevant data for free for research and publish relevant articles. Our study is based on open-source data and does not involve human or animal experiments, so there are no ethical issues.

Consent for publication

Not applicable.

Declaration of competing interest

The authors declare that they have no known competing financial interests or personal relationships that could have appeared to influence the work reported in this paper.

Acknowledgements

The authors would like to thank all individuals who participated in this study.

Abbreviations

LUAD	lung adenocarcinoma
ARLs	anoikis-related lncRNAs
RNA-seq	RNA sequencing
TCGA	The Cancer Genome Atlas
ARGs	anoikis-related genes
MSigDB	Molecular Signatures Database
TMB	tumour mutation burden
qRT−PCR	quantitative real-time PCR
IC50	half maximal inhibitory concentration
NSCLC	non-small cell lung cancer
ECM	extracellular matrix
FPKM	fragments per kilobase of exon model per million mapped reads
TPM	transcripts per kilobase of exon model per million mapped reads
KEGG	Kyoto Encyclopedia of Genes and Genomes
GO	Gene Ontology
GSEA	gene set enrichment analysis
GDSC	Genomics of Drug Sensitivity in Cancer

DEGs	differentially expressed genes
BP	biological process
CC	cellular component
MF	molecular function
TME	tumour microenvironment

Appendix A. Supplementary data

Supplementary data to this article can be found online at https://doi.org/10.1016/j.heliyon.2023.e22200.

References

[1] H. Guo, et al., Microbes in lung cancer initiation, treatment, and outcome: boon or bane? Semin. Cancer Biol. 86 (Pt 2) (2022) 1190–1206.
[2] A.A. Thai, et al., Lung cancer, Lancet 398 (10299) (2021) 535–554.
[3] S. Khadirnaikar, et al., A greedy algorithm-based stem cell LncRNA signature identifies a novel subgroup of lung adenocarcinoma patients with poor prognosis, Front. Oncol. 10 (2020) 1203.
[4] A.S. Lamort, et al., Prognostic phenotypes of early-stage lung adenocarcinoma, Eur. Respir. J. 60 (1) (2022).
[5] F.R. Hirsch, et al., Lung cancer: current therapies and new targeted treatments, Lancet 389 (10066) (2017) 299–311.
[6] S. Yerukala Sathipati, S.Y. Ho, Identifying the miRNA signature associated with survival time in patients with lung adenocarcinoma using miRNA expression profiles, Sci. Rep. 7 (1) (2017) 7507.
[7] C. Bian, et al., A novel glycosyltransferase-related lncRNA signature correlates with lung adenocarcinoma prognosis, Front. Oncol. 12 (2022), 950783.
[8] A.P. Gilmore, Anoikis. Cell Death Differ 12 (Suppl 2) (2005) 1473–1477.
[9] Z. Sun, et al., Identification and validation of an anoikis-associated gene signature to predict clinical character, stemness, IDH mutation, and immune filtration in glioblastoma, Front. Immunol. 13 (2022), 939523.
[10] S. Zhao, et al., A bioinformatics-based analysis of an anoikis-related gene signature predicts the prognosis of patients with low-grade gliomas, Brain Sci. 12 (10) (2022).
[11] Z. Chen, et al., A novel anoikis-related prognostic signature associated with prognosis and immune infiltration landscape in clear cell renal cell carcinoma, Front. Genet. 13 (2022), 1039465.
[12] X. Guan, Cancer metastases: challenges and opportunities, Acta Pharm. Sin. B 5 (5) (2015) 402–418.
[13] N.D. Amoedo, M.F. Rodrigues, F.D. Rumjanek, Mitochondria: are mitochondria accessory to metastasis? Int. J. Biochem. Cell Biol. 51 (2014) 53–57.
[14] D. Fanfone, et al., Confined migration promotes cancer metastasis through resistance to anoikis and increased invasiveness, Elife (2022) 11.
[15] E. Kakavandi, et al., Anoikis resistance and oncoviruses, J. Cell. Biochem. 119 (3) (2018) 2484–2491.
[16] R. Di Micco, et al., Cellular senescence in ageing: from mechanisms to therapeutic opportunities, Nat. Rev. Mol. Cell Biol. 22 (2) (2021) 75–95.
[17] Y. Yu, et al., CircCEMIP promotes anoikis-resistance by enhancing protective autophagy in prostate cancer cells, J. Exp. Clin. Cancer Res. 41 (1) (2022) 188.
[18] Y.N. Kim, et al., Anoikis resistance: an essential prerequisite for tumor metastasis, Int J Cell Biol 2012 (2012), 306879.
[19] T. Tian, et al., CPT1A promotes anoikis resistance in esophageal squamous cell carcinoma via redox homeostasis, Redox Biol. 58 (2022), 102544.
[20] L.N. Wang, et al., TGF-beta1/SH2B3 axis regulates anoikis resistance and EMT of lung cancer cells by modulating JAK2/STAT3 and SHP2/Grb2 signaling pathways, Cell Death Dis. 13 (5) (2022) 472.
[21] Q. Meng, et al., Arginine methylation of MTHFD1 by PRMT5 enhances anoikis resistance and cancer metastasis, Oncogene 41 (32) (2022) 3912–3924.
[22] Z. Shonibare, et al., Reciprocal SOX2 regulation by SMAD1-SMAD3 is critical for anoikis resistance and metastasis in cancer, Cell Rep. 40 (4) (2022), 111066.
[23] A.B. Herman, D. Tsitsipatis, M. Gorospe, Integrated lncRNA function upon genomic and epigenomic regulation, Mol. Cell. 82 (12) (2022) 2252–2266.
[24] E.A. Gibb, C.J. Brown, W.L. Lam, The functional role of long non-coding RNA in human carcinomas, Mol. Cancer 10 (2011) 38.
[25] X. Mo, et al., A novel cuproptosis-related prognostic lncRNA signature and lncRNA MIR31HG/miR-193a-3p/TNFRSF21 regulatory axis in lung adenocarcinoma, Front. Oncol. 12 (2022), 927706.
[26] Y. Wang, et al., Characterization and validation of a ferroptosis-related LncRNA signature as a novel prognostic model for lung adenocarcinoma in tumor microenvironment, Front. Immunol. 13 (2022), 903758.
[27] L. Statello, et al., Gene regulation by long non-coding RNAs and its biological functions, Nat. Rev. Mol. Cell Biol. 22 (2) (2021) 96–118.
[28] Y. Shen, S. Wang, Y. Wu, A novel m6A-related LncRNA signature for predicting prognosis, chemotherapy and immunotherapy response in patients with lung adenocarcinoma, Cells 11 (15) (2022).
[29] J. Ouyang, et al., Long non-coding RNAs are involved in alternative splicing and promote cancer progression, Br. J. Cancer 126 (8) (2022) 1113–1124.
[30] J. Sun, et al., A potential prognostic long non-coding RNA signature to predict metastasis-free survival of breast cancer patients, Sci. Rep. 5 (2015), 16553.
[31] J.Z. Wang, et al., A genetic variant in long non-coding RNA MALAT1 associated with survival outcome among patients with advanced lung adenocarcinoma: a survival cohort analysis, BMC Cancer 17 (1) (2017) 167.
[32] H.L. Cao, et al., lncRNA-RMRP promotes proliferation, migration and invasion of bladder cancer via miR-206, Eur. Rev. Med. Pharmacol. Sci. 23 (3) (2019) 1012–1021.
[33] K. Yuan, et al., Long noncoding RNA TLNC1 promotes the growth and metastasis of liver cancer via inhibition of p53 signaling, Mol. Cancer 21 (1) (2022) 105.
[34] Y.T. Chen, et al., Modular scaffolding by lncRNA HOXA10-AS promotes oral cancer progression, Cell Death Dis. 13 (7) (2022) 629.
[35] L. Jin, et al., The PLAG1-GDH1 Axis promotes anoikis resistance and tumor metastasis through CamKK2-AMPK signaling in LKB1-deficient lung cancer, Mol. Cell. 69 (1) (2018) 87–99 e7.
[36] Y.N. Wang, et al., CPT1A-mediated fatty acid oxidation promotes colorectal cancer cell metastasis by inhibiting anoikis, Oncogene 37 (46) (2018) 6025–6040.
[37] G. Ye, et al., Nuclear MYH9-induced CTNNB1 transcription, targeted by staurosporin, promotes gastric cancer cell anoikis resistance and metastasis, Theranostics 10 (17) (2020) 7545–7560.
[38] J. Zhang, et al., Genome-wide CRISPR/Cas9 library screen identifies PCMT1 as a critical driver of ovarian cancer metastasis, J. Exp. Clin. Cancer Res. 41 (1) (2022) 24.
[39] M. Vivo, et al., p14ARF interacts with the focal adhesion kinase and protects cells from anoikis, Oncogene 36 (34) (2017) 4913–4928.
[40] M.A. Hasnat, et al., Apigenin attenuates melanoma cell migration by inducing anoikis through integrin and focal adhesion kinase inhibition, Molecules 20 (12) (2015) 21157–21166.
[41] M. Enkhbat, et al., Harnessing focal adhesions to accelerate p53 accumulation and anoikis of A549 cells using colloidal self-assembled patterns (cSAPs), ACS Appl. Bio Mater. 5 (1) (2022) 322–333.
[42] Z. Zhou, et al., AEG-1 promotes anoikis resistance and orientation chemotaxis in hepatocellular carcinoma cells, PLoS One 9 (6) (2014), e100372.
[43] F. Macabenta, H.T. Sun, A. Stathopoulos, BMP-gated cell-cycle progression drives anoikis during mesenchymal collective migration, Dev. Cell 57 (14) (2022) 1683–1693 e3.

[44] C. Shen, et al., LncRNA GASAL1 promotes hepatocellular carcinoma progression by up-regulating USP10-stabilized PCNA, Exp. Cell Res. 415 (1) (2022), 112973.
[45] J. Liu, Q. Zhang, N. Ma, LncRNA GASAL1 interacts with SRSF1 to regulate trophoblast cell proliferation, invasion, and apoptosis via the mTOR signaling pathway, Cell Transplant. 29 (2020), 963689720965182.
[46] Y. Zhu, et al., A computed tomography (CT)-derived radiomics approach for predicting primary co-mutations involving TP53 and epidermal growth factor receptor (EGFR) in patients with advanced lung adenocarcinomas (LUAD), Ann. Transl. Med. 9 (7) (2021) 545.
[47] H. Sun, et al., Specific TP53 subtype as biomarker for immune checkpoint inhibitors in lung adenocarcinoma, EBioMedicine 60 (2020), 102990.